Nodeless superconductivity in β-$PdBi_2$

Jian Chen,[1,*] An Wang,[2] Guiming Pang,[2] Hang Su,[2] Ye Chen,[2] and Huiqiu Yuan[2,3,†]
[1]*Zhejiang University of Water Resources and Electric Power, Hangzhou, Zhejiang 310018, China*
[2]*Center for Correlated Matter and Department of Physics, Zhejiang University, Hangzhou, Zhejiang 310058, China*
[3]*Collaborative Innovation Center of Advanced Microstructures, Nanjing University, Nanjing 210093, China*

(Received 4 November 2019; revised manuscript received 8 February 2020; accepted 10 February 2020; published 25 February 2020)

The superconducting gap symmetry of β-$PdBi_2$ is studied by measuring the London penetration depth $\Delta\lambda(T)$ as well as the heat capacity $C_P(T, B)$. In the low temperature limit, both the penetration depth $\Delta\lambda(T)$ and the electronic specific heat $C_e(T)/T$ follow exponential-type temperature dependence, providing evidence for fully gapped superconductivity in this compound. Analysis of the superfluid density $\rho_s(T)$ suggests single-gap s-wave superconductivity for β-$PdBi_2$, which is further supported by the linear field dependence of the Sommerfeld coefficient $\gamma_0(B)$ determined in the superconducting state.

DOI: 10.1103/PhysRevB.101.054514

I. INTRODUCTION

A topological superconductor (TSC) hosts a fully opened gap in the bulk and a topologically protected gapless surface (or edge) state which is essentially zero-energy Andreev bound state consisting of Majorana fermions at the vortex core center [1]. The Majorana fermions, their own antiparticles, are not only of scientific interest for fundamental physics, but also potential candidates for applications in spintronics and quantum computation [2,3]. Compared with other TSC candidates which are achieved exclusively by a carrier doping, e.g., Cu-intercalated Bi_2Se_3 [4–7] and In-doped SnTe [8,9], or by applying pressure, e.g., M_2Te_3 (M = Bi, Sb) [10,11], the recently discovered TSC candidate β-$PdBi_2$ has attracted great attentions because it is in a pure stoichiometric ratio with a relatively high T_c (~4.25 K) [12] and hosts robust superconductivity to variant dopants and pressure [13,14]. Besides β-$PdBi_2$, several superconducting phases have been reported in Pd-Bi binary systems: noncentrosymmetric (NCS) α-PdBi ($T_c \sim 3.8$ K) [15], α-$PdBi_2$ ($T_c \sim 1.7$ K) [16], and γ-$Pd_{2.5}Bi_{1.5}$ ($T_c \sim 3.7$ K) [17]. Among them, β-$PdBi_2$ crystallizes in a centrosymmetric tetragonal structure with the space group of $I4/mmm$ [12]. Band structure calculations show two holelike and two electronlike pockets formed by Bi-6p and Pd-4d bands at the Fermi level (E_F) which are already inverted without spin-orbit coupling (SOC) [18,19]. Thus, β-$PdBi_2$ could be a promising platform to realize topological superconductivity and may offer a rare opportunity to explore Majorana fermions.

There are extensive studies on the superconducting pairing symmetry for β-$PdBi_2$. Spin- and angle-resolved photoemission spectroscopy (ARPES) and quasiparticle interference (QPI) imaging measured by scanning tunneling microscopy (STM) have revealed the presence of spin-polarized topological surface states around E_F and a fully opened superconducting gap [18,20]. Moreover, evidence for Majorana bound states is observed at the center of the vortices in epitaxial thin film [21]. Little-Parks experiments performed on textured β-$PdBi_2$ thin film demonstrate the existence of half-quantum flux, suggesting a spin-triplet pairing state [22]. Recently, Kolapo *et al.* provided transport evidence that while the undoped system is a trivial SC, K-doped β-$PdBi_2$ is a three-dimensional time-reversal-invariant topological SC [23]. An unprecedented topological quantum phase transition in the superconducting state is thus suggested. On the other hand, conventional s-wave superconductivity is suggested from calorimetric studies as well as other tunneling experiments, muon spin relaxation (μSR), and point-contact spectroscopy on bulk samples [24–27]. However, it is still not clear whether it possesses a single gap [25] or multiple energy gaps [12] in the bulk superconductivity, as inferred from the specific heat data measured in different groups. It is therefore highly desired to further characterize the superconducting pairing state of β-$PdBi_2$ using other experimental techniques.

In this article we report the low-temperature measurements of London penetration depth $\Delta\lambda(T)$ and the heat capacity $C_P(T, B)$ for β-$PdBi_2$. Our results demonstrate strong evidence for fully gapped superconductivity.

II. EXPERIMENTAL METHODS

Single crystals of β-$PdBi_2$ were synthesized via a melt-growth method as discussed in Refs. [18,24]. The starting materials of Bi powder (99.99%, Alfa Aesar) and Pd powder (99.95%, Alfa Aesar), with a prescribed molar ratio of Bi:Pd = 2:1 (total: 2 g), were sealed in an evacuated quartz tube. This quartz tube was heated at 900 °C for 24 h, slowly cooled down to 490 °C in 96 h, and then to 395 °C in 200 h. To avoid formation of the α-$PdBi_2$ phase which stabilizes below 380 °C, we quenched the crystals from 395 °C down to room temperature in ice water. The obtained single crystals have a good cleavage, producing flat surfaces as large as

*chenjian123@zju.edu.cn
†hqyuan@zju.edu.cn

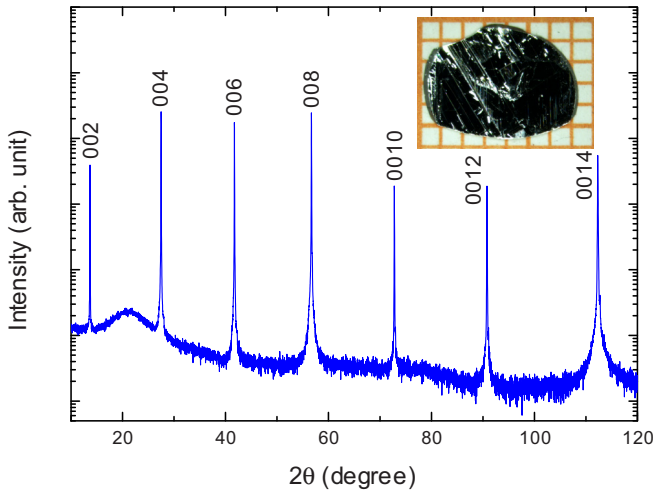

FIG. 1. X-ray diffraction of the β-$PdBi_2$ single crystal. An image of the sample is shown in the inset. The square size on the background grid is 1×1 mm^2.

$\sim 5 \times 5$ mm^2, see the inset of Fig. 1. The main panel of Fig. 1 shows the x-ray diffraction (XRD) of a β-$PdBi_2$ single crystal using Cu $K\alpha$ radiation at room temperature. All these patterns can be indexed with a tetragonal unit cell with the space group of $I4/mmm$. No impurity phase was presented and [001] crystallographic orientation of the tetragonal lattice can be confirmed with interlayer spacing $c = 12.96$ Å, in good agreement with previous reports [12,24]. Sample compositions were identified by using energy dispersive x-ray spectroscopy (EDS) as Pd:Bi $= (1.00 \pm 0.03) : (1.87 \pm 0.04)$, which are close to the nominal values.

The electrical resistivity was measured using a standard four-probe method. Measurements of the magnetic susceptibility and specific heat were performed in a commercial magnetic property measurement system (MPMS-5T) and a physical property measurement system (PPMS-9T) (Quantum Design), respectively. Measurements of the penetration depth change $\Delta\lambda(T)$ were performed by utilizing a tunnel diode oscillator (TDO) based self-inductance technology [28] down to a base temperature of 0.35 K in a ^{3}He cryostat with a frequency of 7 MHz and a noise level of about 0.1 Hz. With this method, the change of the London penetration depth $\Delta\lambda(T) = \lambda(T) - \lambda(0)$ is proportional to the resonant frequency shift as $\Delta\lambda(T) = G\Delta f(T)$. Here the calibration constant G is determined from the sample and coil geometries [28].

III. RESULTS AND DISCUSSION

Figure 2 shows the electrical resistivity $\rho(T)$ (a) and magnetic susceptibility $\chi(T)$ (b) of β-$PdBi_2$ near T_c. The presence of a superconducting transition is clearly seen from a sharp drop of the resistivity onsetting around 4.5 K, together with a narrow transition width $\Delta T = 0.2$ K, and also from a diamagnetic signal in the magnetic susceptibility, suggesting bulk superconductivity. Here a demagnetizing factor of $N = 0.22$, estimated from the sample geometry [29], is considered while calculating the magnetic susceptibility $\chi(T)$, which shows

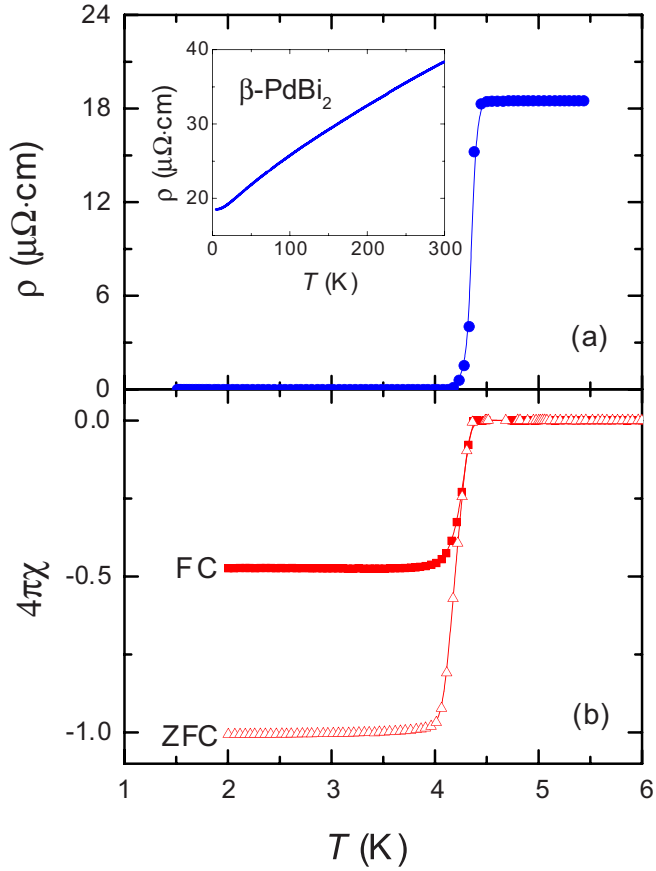

FIG. 2. The main panel shows data of β-$PdBi_2$ near T_c: (a) electrical resistivity $\rho(T)$ and (b) magnetic susceptibility $\chi(T)$ under a magnetic field of 10 Oe applied parallel to the *ab* plane, at zero-field cooling (ZFC) and field cooling (FC) mode, respectively. Inset to (a) plots the normal state electrical resistivity $\rho(T)$ at zero field in the temperature range of $T = 5$–300 K with current flowing within the *ab* plane.

nearly perfect diamagnetism in the superconducting state. The inset of Fig. 2(a) presents $\rho(T)$ between 5 and 300 K at $B = 0$, which shows simple metallic behavior in the normal state. The residual resistivity of 18.5 $\mu\Omega$ cm is in the same order of magnitude with those reported in literature [12,18,24,27]. Following the method in Ref. [30], we estimated a mean free path of $l \approx 4000$ Å using the coherence length $\xi(0) \approx 230$ Å from calorimetric measurements [25] as well as resistivity $\rho(T_c) = 18.5$ $\mu\Omega$ cm, normal-state Sommerfeld coefficient $\gamma_n = 5.40$ mJ/mol K^2, and $T_c = 4.5$ K from our data. The derived mean free path is therefore much larger than the coherence length ξ, suggesting that our sample is in the clean limit.

London penetration depth is an important parameter to characterize the superconducting pairing symmetry. In the low temperature limit, the penetration depth $\Delta\lambda(T)$ shows exponential type of temperature dependence for fully gapped superconductivity, but power-law behavior in the case of nodal superconductivity. In Fig. 3, temperature dependence of the penetration depth change $\Delta\lambda(T)$ of β-$PdBi_2$ is shown for sample 1 ($T_c = 4.45$ K) and sample 2 ($T_c = 4.5$ K), which are cut from different batches. As an example, the inset of

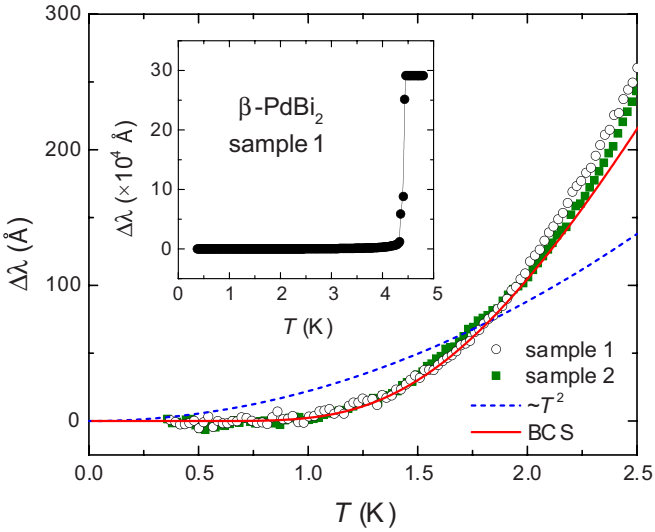

FIG. 3. Low-temperature in-plane penetration depth $\Delta\lambda(T)$ of β-$PdBi_2$ for two samples: 1 (circles) and 2 (squares). The solid and dashed lines represent the fits of experimental data to power law of T^2 and BCS model of Eq. (1) below $\sim 0.4T_c$, respectively. Inset shows $\Delta\lambda(T)$ for sample 1 at temperatures of 0–5 K.

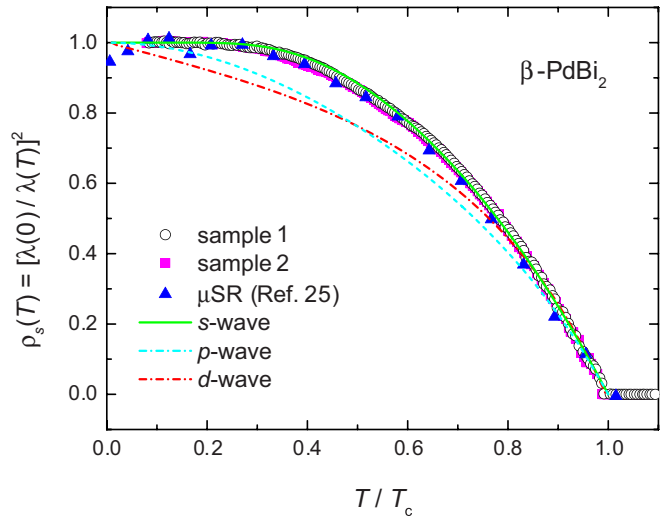

FIG. 4. In-plane superfluid density ρ_s plotted in the normalized temperature scale for β-$PdBi_2$: sample 1 (circles) and 2 (squares), together with the normalized μSR data [26] (triangles). Solid, dashed, and dashed-dotted lines are the fits of the experimental data using single-gap BCS s-wave, p-wave, and two-dimensional d-wave pairing states, respectively (see context).

Fig. 3 shows the London penetration depth change $\Delta\lambda(T)$ of sample 1 over a wider temperature range from 5 K above T_c down to about 0.35 K. A sharp superconducting transition with $T_c = 4.45$ K is observed, which is in good agreement with the values derived from the resistivity and magnetization measurements. The main panel of Fig. 3 presents the penetration depth below 2.5 K, which exhibits a weak temperature dependence at low temperatures, suggesting fully gapped superconductivity. As shown in this plot, this behavior is well producible between the two samples. The power-law behavior of $\Delta\lambda(T) \sim T^n$ with $n = 1$ or 2 fails to illustrate $\Delta\lambda(T)$ data (see the dashed line in Fig. 3), excluding nodal superconductivity for β-$PdBi_2$. For an s-wave SC at $T \ll T_c$ [31], $\Delta\lambda(T)$ can be approximated by

$$\Delta\lambda(T) = \lambda(0)\sqrt{\frac{\pi\Delta(0)}{2T}}\exp\left[-\frac{\Delta(0)}{T}\right], \tag{1}$$

where $\lambda(0)$ and $\Delta(0)$ are the penetration depth and superconducting gap amplitude at zero temperature, respectively (in units with $k_B = 1$). Here $\lambda(0) = 2630$ Å is determined from the transverse field μSR experiments [26]. In Fig. 3, the dashed line shows the best fit of our experimental data $\Delta\lambda(T)$ to the BCS model for $T \leqslant 0.4T_c$, with the fitting parameter $\Delta(0) = 1.85T_c$. The fitted gap values are well consistent for both samples.

To further characterize the superconducting pairing state of β-$PdBi_2$, we also analyze the in-plane normalized superfluid density, which was converted from $\lambda(T)$ using $\rho_s(T) = [\lambda(0)/\lambda(T)]^2$. Here $\lambda(T) = \lambda(0) + \Delta\lambda(T)$, with a fixed value of $\lambda(0) = 2630$ Å [26]. In the main panel of Fig. 4 we plot the derived superfluid density $\rho_s(T)$ versus the normalized temperature T/T_c for sample 1 and sample 2. We analyze our superfluid density $\rho_s(T)$ in terms of a single-gap s-wave model in the clean limit [32], i.e.,

$$\rho_s(T) = 1 + 2\left\langle\int_{\Delta_k}^{\infty}\frac{\partial f}{\partial E}\frac{E}{\sqrt{E^2-\Delta_k^2}}dE\right\rangle_{\rm FS}, \tag{2}$$

where $f(E,T) = [1+\exp(E/T)]^{-1}$ denotes the Fermi distribution function and $\langle\cdots\rangle_{\rm FS}$ represents an average over the Fermi surface. The superconducting gap function is defined as $\Delta_k(T) = \Delta(T)g_k$, with an angular-dependent parameter $g_k = 1$, $\sin\theta$, and $\cos 2\phi$ for the s-, p-, and d-wave models, respectively, where θ is the polar angle and ϕ is the azimuthal angle. The temperature dependence of the gap $\Delta(T)$ is approximated as [33]

$$\Delta(T) = \Delta(0)\tanh\left\{1.82\left[1.018\left(\frac{T_c}{T}-1\right)\right]^{0.51}\right\}. \tag{3}$$

Here the zero temperature gap magnitude $\Delta(0)$ is the only adjustable parameter in the fitting. As shown in Fig. 4, $\rho_s(T)$ of β-$PdBi_2$ can be nicely fitted by the s-wave model as described above (solid line): $\Delta(0) = 2.0T_c$ for sample 1 and $\Delta(0) = 1.98T_c$ for sample 2, respectively. The gap magnitude is larger than the value of $1.76T_c$ for weakly coupled BCS SC, suggesting moderately strong coupling for β-$PdBi_2$. Furthermore, the $\rho_s(T)$ data from the μSR experiments [26] are also included, which overlap well with our data from the TDO measurements. The so-obtained gap magnitude $\Delta(0)$ agrees well with the values derived from our fits to the penetration depth and the specific heat data discussed below. On the other hand, two nodal superconducting scenarios are also displayed for comparison: spin-triplet p-wave model [34] with point nodes (dashed line) and spin-singlet d-wave model [28] with line nodes (dashed-dotted line). Since the superfluid density becomes saturated at low temperatures below around $0.25T_c$, it is obvious from Fig. 4 that the nodal gap functions cannot

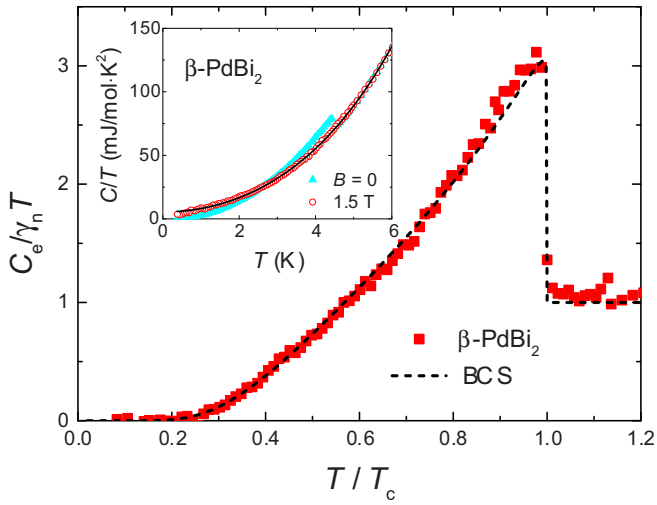

FIG. 5. The main panel shows the electronic specific heat $C_e(T)/\gamma_n T$ vs T/T_c for β-$PdBi_2$ after subtracting the phonon contributions. Dashed line: The fit to the BCS model with $\Delta_0 = 2.05T_c$. Inset shows $C(T)/T$ measured at $B = 0$ (triangles) and 1.5 T (circles), respectively. Solid line: The power-law fitting (see context) in the temperature range of 1–6 K.

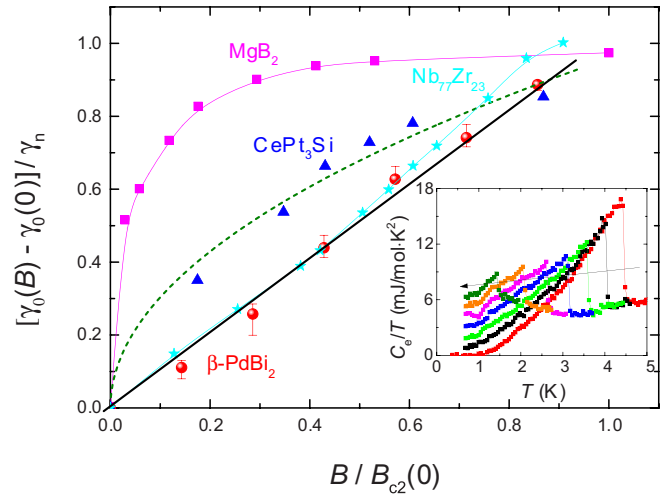

FIG. 6. The main panel shows the magnetic field dependence of the normalized Sommerfeld coefficient for β-$PdBi_2$, plotted as $[\gamma_0(B) - \gamma_0(0)]/\gamma_n$ versus $B/B_{c2}(0)$ for β-$PdBi_2$ (this work, circles with error bars), MgB_2 [39] (squares), $CePt_3Si$ for $B\|[100]$ [40] (triangles), and $Nb_{77}Zr_{23}$ [41] (stars), respectively. Solid lines are guides to the eyes, while the dashed line is a square-root fitting (see the context). Inset shows the evolution of $C_e(T)/T$ with the applied magnetic fields of $B = 0$–0.6 T, which increases along the arrow direction.

describe the experimental data, of which the superfluid density show strong temperature dependence due to the existence of low energy excitations. Therefore, our measurements of the penetration depth give strong evidence for single-gap s-wave superconductivity in β-$PdBi_2$.

Temperature dependence of the specific heat $C(T)$ for β-$PdBi_2$ was previously reported by two groups, independently. Both show exponential behavior at low temperatures, but are fitted with different gap functions, i.e., one-gap [25] versus two-gap [12] BCS superconductivity. In order to clarify this uncertainty and then compare it with the penetration depth, we remeasured the heat capacity of β-$PdBi_2$, both at zero and applied magnetic field. The inset of Fig. 5 plots the specific heat of β-$PdBi_2$ at $B = 0$ [$C_0(T)$, triangles] and 1.5 T [$C_{1.5T}(T)$, circles]. At zero field, the superconducting transition is observed at $T_c = 4.48$ K, which is consistent with our transport and penetration depth measurements. At $B = 1.5$ T, larger than the upper critical field from Ref. [25], one can see that bulk superconducting transition is suppressed below our base temperature. The specific heat data at $B = 1.5$ T can be nicely fitted by the polynomial expression: $C_{1.5T}(T) = \gamma_n T + (B_3T^3 + B_5T^5)$, in which $\gamma_n T$ and $C_{ph} = (B_3T^3 + B_5T^5)$ represent the normal-state electronic and phonon contributions, respectively. The normal-state Sommerfeld coefficient $\gamma_n = 5.40$ mJ/mol K^2 is thus obtained. The electronic heat capacity in the superconducting state can be therefore obtained by subtracting the field-independent phonon contribution C_{ph} from the total heat capacity by $C_e(T, B) = C(T, B) - C_{ph}(T)$. The main panel of Fig. 5 plots the so-derived electronic heat capacity $C_e/\gamma_n T$ vs T/T_c near the superconducting transition, which is well consistent with data from Ref. [25], showing a very weak temperature dependence far below the superconducting transition ($T < 0.3T_c$). The specific heat jump at T_c, i.e., $\Delta C/\gamma_n T_c = 1.97$, is larger than the BCS value of 1.43, suggesting strong coupling for β-$PdBi_2$ [35]. Following the procedures described in Ref. [36], $C_e(T)$ data, as well as the superconducting jump, is well fitted by the one-gap α model with an energy gap of $\Delta(0) = 2.05T_c$. This is consistent with the above penetration depth and superfluid density results and indicates a moderately enhanced superconducting gap magnitude.

We further characterize the superconducting pairing state of β-$PdBi_2$ by measuring the specific heat $C(T)$ at various magnetic fields. The residual Sommerfeld coefficient $\gamma_0(B)$ in the superconducting state gives important information about the low-energy excitations which exist near the Abrikosov vortex line. In a fully gapped SC, the low-lying excitations are usually confined to the vortex cores in the normal state, and the residual Sommerfeld coefficient is proportional to the vortex density which is a linear function of the applied magnetic field [37], i.e., $\gamma_0(B) \sim B$. On the other hand, for a highly anisotropic SC or SC with nodes in the energy gap, the quasiparticle excitations can spread outside the vortex cores, contributing significantly to the specific heat over the cores themselves at low temperatures. Volovik predicted that [38] in a nodal SC, a Doppler shift on the excitation energy may result in a square-root field dependence of the residual Sommerfeld coefficient, i.e., $\gamma_0(B) \propto B^{1/2}$. Figure 6 presents the magnetic field dependence of the normalized Sommerfeld coefficient, plotted as $[\gamma_0(B) - \gamma_0(0)]/\gamma_n$ versus $B/B_{c2}(0)$ for β-$PdBi_2$ (circles). Here the values of C_e/T at 0.68 K (the lowest temperature measured) for $B > 0$ and 0.37 K for $B = 0$ are taken as γ_0. For comparison, we also plot the data previously reported for MgB_2 [39] (squares), $CePt_3Si$ for $B\|[100]$ [40] (triangles), and $Nb_{77}Zr_{23}$ [41] (stars), respectively. One can see that $\gamma_0(B)$ of β-$PdBi_2$, similar to that of the BCS SC $Nb_{77}Zr_{23}$ [41], increases linearly with increasing the applied magnetic field, clearly deviating either from the behavior of

the two-band SC MgB_2 [39], which increases fast at low fields before saturating at high fields near $B_{c2}(0)$, or from the square-root field dependence ($[\gamma_0(B) - \gamma_0(0)]/\gamma_n = 0.95[B/B_{c2}(0)]$, see the dashed line) of the heavy-fermion NCS SC $CePt_3Si$ [40], providing further evidence for single-gap *s*-wave superconductivity for β-$PdBi_2$.

As shown above, all our measurements consistently demonstrate fully gapped superconductivity for β-$PdBi_2$, which can be well described by a single-gap BCS model. The obtained superconducting gap $\Delta(0) \sim 1.85-2.05T_c$, determined either from the bulk calorimetric measurements or the penetration depth, is in full agreement with the previous measurements from Hall-probe magnetometry [25] and point contact Andreev reflection spectroscopy [27], but larger than the values (0.76–0.8 meV $\approx 1.70-1.85T_c$) derived from the spectroscopic measurements of μSR [26], STM [24], and QPI [20]. The reason for differences in the superconducting gap is likely attributed to the variance of T_c which might be affected by the sample quality [12].

The large spin-orbit coupling in Pd-Bi binaries has stimulated extensive investigations on the possible topological surface states. Among the superconducting Pd-Bi family, unlike α-$PdBi_2$ and β-$PdBi_2$ which are both centrosymmetric, α-PdBi lacks an inversion center. Rashba-type antisymmetric spin-orbit coupling in NCS SC α-PdBi can lift the spin degeneracy and lead to a mixed pairing of both spin-singlet and spin-triplet superconductivity [42]. Spin-polarized surface state at high-binding energy for α-PdBi was experimentally observed from a spin-resolved ARPES study [43]. Low-energy surface states that develop from Rashba splitting in close proximity to the Fermi energy for α-$PdBi_2$ are identified, providing the potential signature of Majorana fermions [44]. Although extensive theoretical and experimental studies have provided the existence of topological surface states in Pd-Bi binaries [18,20,43,44], fully gapped *s*-wave (singlet) superconductivity is demonstrated in the bulk measurements [45], being similar to the case of $PbTaSe_2$ with a NCS structure, which was also proposed as a candidate of TSC [46]. In $PbTaSe_2$, band structure calculations reveal nodal lines [47] and STM experiments show a zero bias peak at the vortex core [48]. Measurements of penetration depth suggest fully gapped superconductivity [49], exactly similar to what we observed here in β-$PdBi_2$. More recently, evidence for nematic superconductivity with a clear twofold symmetry while rotating the magnetic field in the *ab* plane was clearly observed in the soft point-contact zero bias conductance and the resistive upper critical field, but is absent in the bulk measurements [50]. This is in contrast to the doped topological insulators $Cu_xBi_2Se_3$, $Sr_xBi_2Se_3$, and $Nb_xBi_2Se_3$, where nematic superconductivity is evidenced in the bulk properties: rotation symmetry breaking in spin rotation and superconducting gap amplitude [51]. Therefore, it might be very interesting to perform similar experiments on β-$PdBi_2$, which might help elucidate the possible existence of topological superconductivity in this compound.

IV. CONCLUSION

In summary, we have studied the superconducting gap symmetry of β-$PdBi_2$ single crystals by measuring the London penetration depth $\Delta\lambda(T)$ as well as the heat capacity $C(T, B)$ at low temperatures. The temperature dependence of the penetration depth $\Delta\lambda(T)$, the superfluid density $\rho_s(T)$, as well as the electronic specific heat $C_e(T)/T$ can be consistently described by a single-gap BCS model. The Sommerfeld coefficient follows a linear field dependence as $\gamma_0(B) \sim B$. All these findings suggest that β-$PdBi_2$ behaves like a fully gapped superconductor with a moderately enhanced superconducting gap magnitude.

ACKNOWLEDGMENTS

We appreciate valuable discussions with X. Lu. This work was supported by the National Natural Science Foundation of China (Grants No. 11974306 and No. U1632275), the National Key R&D Program of China (Grants No. 2016YFA0300202 and No. 2017YFA0303100), the Zhejiang Provincial Natural Science Foundation of China (Grant No. LQ19A040006), and the Science and technology project of Water Conservancy Department of Zhejiang Province (Grant No. RC1994).

[1] X. L. Qi and S. C. Zhang, Rev. Mod. Phys. **83**, 1057 (2011).
[2] F. Wilczek, Nat. Phys. **5**, 614 (2009).
[3] C. Beenakker, Annu. Rev. Condens. Matter Phys. **4**, 113 (2013).
[4] Y. S. Hor, A. J. Williams, J. G. Checkelsky, P. Roushan, J. Seo, Q. Xu, H. W. Zandbergen, A. Yazdani, N. P. Ong, and R. J. Cava, Phys. Rev. Lett. **104**, 057001 (2010).
[5] L. Fu and E. Berg, Phys. Rev. Lett. **105**, 097001 (2010).
[6] M. Kriener, K. Segawa, Z. Ren, S. Sasaki, and Y. Ando, Phys. Rev. Lett. **106**, 127004 (2011).
[7] S. Sasaki, M. Kriener, K. Segawa, K. Yada, Y. Tanaka, M. Sato, and Y. Ando, Phys. Rev. Lett. **107**, 217001 (2011).
[8] M. Novak, S. Sasaki, M. Kriener, K. Segawa, and Y. Ando, Phys. Rev. B **88**, 140502(R) (2013).
[9] S. Sasaki, Z. Ren, A. A. Taskin, K. Segawa, L. Fu, and Y. Ando, Phys. Rev. Lett. **109**, 217004 (2012).
[10] J. L. Zhang, S. J. Zhang, H. M. Weng, W. Zhang, L. X. Yang, Q. Q. Liu, S. M. Feng, X. C. Wang, R. C. Yu, L. Z. Cao, L. Wang, W. G. Yang, H. Z. Liu, W. Y. Zhao, S. C. Zhang, X. Dai, Z. Fang, and C. Q. Jin, Proc. Natl. Acad. Sci. USA **108**, 24 (2011).
[11] J. Zhu, J. L. Zhang, P. P. Kong, S. J. Zhang, X. H. Yu, J. L. Zhu, Q. Q. Liu, X. Li, R. C. Yu, R. Ahuja, W. G. Yang, G. Y. Shen, H. K. Mao, H. M. Weng, X. Dai, Z. Fang, Y. S. Zhao, and C. Q. Jin, Sci. Rep. **3**, 2016 (2013).
[12] Y. Imai, F. Nabeshima, T. Yoshinaka, K. Miyatani, R. Kondo, S. Komiya, I. Tsukada, and A. Maeda, J. Phys. Soc. Jpn. **81**, 113708 (2012).
[13] K. Zhao, B. Lv, Y. Y. Xue, X. Y. Zhu, L. Z. Deng, Z. Wu, and C. W. Chu, Phys. Rev. B **92**, 174404 (2015).
[14] G. Pristáš, Mat. Orendáč, S. Gabáni, J. Kačmarčík, E. Gažo, Z. Pribulová, A. Correa-Orellana, E. Herrera, H. Suderow, and P. Samuely, Phys. Rev. B **97**, 134505 (2018).
[15] B. Joshi, A. Thamizhavel, and S. Ramakrishnan, Phys. Rev. B **84**, 064518 (2011).

[16] N. N. Zhuravlev, Zh. Eksp. Teor. Fiz. **32**, 1305 (1957).
[17] B. T. Matthias, T. H. Geballe, and V. B. Compton, Rev. Mod. Phys. **35**, 1 (1963).
[18] M. Sakano, K. Okawa, M. Kanou, H. Sanjo, T. Okuda, T. Sasagawa, and K. Ishizaka, Nat. Commun. **6**, 8595 (2015).
[19] I. R. Shein and A. L. Ivanovskii, J. Supercond. Nov. Magn. **26**, 1 (2013).
[20] K. Iwaya, Y. Kohsaka, K. Okawa, T. Machida, M. S. Bahramy, T. Hanaguri, and T. Sasagawa, Nat. Commun. **8**, 976 (2017).
[21] Y. F. Lv, W. L. Wang, Y. M. Zhang, H. Ding, W. Li, L. Wang, K. He, C. L. Song, X. C. Ma, and Q. K. Xue, Sci. Bull. **62**, 852 (2017).
[22] Y. F. Li, X. Y. Xu, M.-H. Lee, M.-W. Chu, and C. L. Chien, Science **366**, 238 (2019).
[23] A. Kolapo, T. Li, P. Hosur, and J. H. Miller, arXiv:1809.08708.
[24] E. Herrera, I. Guillamón, J. A. Galvis, A. Correa, A. Fente, R. F. Luccas, F. J. Mompean, M. García-Hernández, S. Vieira, J. P. Brison, and H. Suderow, Phys. Rev. B **92**, 054507 (2015).
[25] J. Kačmarčík, Z. Pribulová, T. Samuely, P. Szabó, V. Cambel, J. Šoltýs, E. Herrera, H. Suderow, A. Correa-Orellana, D. Prabhakaran, and P. Samuely, Phys. Rev. B **93**, 144502 (2016).
[26] P. K. Biswas, D. G. Mazzone, R. Sibille, E. Pomjakushina, K. Conder, H. Luetkens, C. Baines, J. L. Gavilano, M. Kenzelmann, A. Amato, and E. Morenzoni, Phys. Rev. B **93**, 220504(R) (2016).
[27] L. Che, T. Le, C. Q. Xu, X. Z. Xing, Z. Shi, X. Xu, and X. Lu, Phys. Rev. B **94**, 024519 (2016).
[28] R. Prozorov and R. W. Giannetta, Supercond. Sci. Technol. **19**, R41 (2006).
[29] E. H. Brandt, Phys. Rev. B **60**, 11939 (1999).
[30] T. P. Orlando, E. J. McNiff, Jr., S. Foner, and M. R. Beasley, Phys. Rev. B **19**, 4545 (1979).
[31] B. Muhlschlegel, Z. Phys. **155**, 313 (1959).
[32] M. Tinkham, *Introduction to Superconductivity*, 2nd ed, (McGraw-Hill, New York, 1996).
[33] A. Carrington and F. Manzano, Physica C **385**, 205 (2003).
[34] A. Bhattacharyya, D. T. Adroja, J. Quintanilla, A. D. Hillier, N. Kase, A. M. Strydom, and J. Akimitsu, Phys. Rev. B **91**, 060503(R) (2015).
[35] H. Matsuzaki, K. Nagai, N. Kase, T. Nakano, and N. Takeda, J. Phys.: Conf. Series **871**, 012004 (2017).
[36] H. Padamsee, J. E. Neighbor, and C. A. Shiffman, J. Low Temp. Phys. **12**, 387 (1973).
[37] C. Caroli, P. G. de Gennes, and J. Matricon, Phys. Lett. **9**, 307 (1964).
[38] G. E. Volovik, JETP Lett. **58**, 469 (1993).
[39] F. Bouquet, R. A. Fisher, N. E. Phillips, D. G. Hinks, and J. D. Jorgensen, Phys. Rev. Lett. **87**, 047001 (2001).
[40] T. Takeuchi, T. Yasuda, M. Tsujino, H. Shishido, R. Settai, H. Harima, and Y. Ōnuki, J. Phys. Soc. Jpn. **76**, 014702 (2007).
[41] A. Mirmelstein, A. Junod, E. Walker, B. Revaz, Y. Genoud, and G. Triscone, J. Supercond. **10**, 527 (1997).
[42] E. Bauer and M. Sigrist, *Non-Centrosymmetric Superconductors* (Springer, Berlin, 2012).
[43] M. Neupane, N. Alidoust, M. M. Hosen, J. X. Zhu, K. Dimitri, S. Y. Xu, N. Dhakal, R. Sankar, I. Belopolski, D. S. Sanchez, T. R. Chang, H. T. Jeng, K. Miyamoto, T. Okuda, H. Lin, A. Bansil, D. Kaczorowski, F. Chou, M. Z. Hasan, and T. Kurakiewicz, Nat. Commun. **7**, 13315 (2016).
[44] K. Dimitri, M. M. Hosen, G. Dhakal, H. Choi, F. Kabir, C. Sims, D. Kaczorowski, T. Durakiewicz, J. X. Zhu, and M. Neupane, Phys. Rev. B **97**, 144514 (2018).
[45] S. Mitra, K. Okawa, S. Kunniniyil Sudheesh, T. Sasagawa, J.-X. Zhu, and Elbert E. M. Chia, Phys. Rev. B **95**, 134519 (2017).
[46] M. N. Ali, Q. D. Gibson, T. Klimczuk, and R. J. Cava, Phys. Rev. B **89**, 020505(R) (2014).
[47] G. Bian, T. R. Chang, R. Sankar, S. Y. Xu, H. Zheng, T. Neupert, C. K. Chiu, S. M. Huang, G. Chang, I. Belopolski, D. S. Sanchez, M. Neupane, N. Alidoust, C. Liu, B. Wang, C. C. Lee, H. T. Jeng, C. Zhang, Z. Yuan, S. Jia, A. Bansil, F. Chou, H. Lin, and M. Z. Hasan, Nat. Commun. **7**, 10556 (2016).
[48] S. Y. Guan, P. J. Chen, M. W. Chu, R. Sankar, F. C. Chou, H. T. Jeng, C. S. Chang, and T. M. Chuang, Sci. Adv. **2**, e1600894 (2016).
[49] G. M. Pang, M. Smidman, L. X. Zhao, Y. F. Wang, Z. F. Weng, L. Q. Che, Y. Chen, X. Lu, G. F. Chen, and H. Q. Yuan, Phys. Rev. B **93**, 060506(R) (2016).
[50] T. Le, Y. Sun, H. K. Jin, L. Che, L. Yin, J. Li, G. M. Pang, C. Q. Xu, L. X. Zhao, S. Kittaka, T. Sakakibara, K. Machida, R. Sankan, H. Q. Yuan, G. F. Chen, X. F. Xu, S. Y. Li, Y. Zhou, and X. Lu, arXiv:1905.11177.
[51] M. Sato and Y. Ando, Rep. Prog. Phys. **80**, 076501 (2017).